Energy Materials

Article

Tuning wettability of gallium-based liquid metal anode for lithium-ion battery via a metal mixing strategy

Yang Lv , **Honghao Hu, Xizheng Liu***

Tianjin Key Laboratory of Advanced Functional Porous Materials, Institute for New Energy Materials and Low-Carbon Technologies, School of Materials Science and Engineering, Tianjin University of Technology, Tianjin 300380, China.

*Correspondence to: Prof. Xizheng Liu, Tianjin Key Laboratory of Advanced Functional Porous Materials, Institute for New Energy Materials and Low-Carbon Technologies, Tianjin University of Technology, Tianjin 300380, China. E-mail: xzliu@tjut.edu.cn

Abstract

Exploring highly stable alloy-type anodes for rechargeable lithium batteries is urgent with the ever-increasing demands for high energy density batteries. The liquid metal (LM)-based anodes demonstrate great potential in advanced lithium-ion batteries due to their high energy densities and self-healing performance. However, its high surface tension leads to poor wettability towards the current collector and higher interfacial contact resistance. In this study, we developed a new free-standing LM-based anode LM-W10/Cu foil with good wettability and machinability by mixing high-melting-point tungsten (W) nanoparticles. It greatly improves the inherent defects of poor interfacial contact and lithium diffusion kinetics between the LM and current collectors, reduces the tedious and costly electrode manufacturing process, and regulates lithium deposition behaviors. And this metal mixing strategy has a negligible effect on the self-healing nature of LM. Symmetric cells of LM-W10/Cu foil anodes displayed a low overpotential (~13 mV) and cycled stably for more than 8,000 h (4,000 cycles) at 0.5 or 1 mA/cm^2; full cells coupled with LiFePO$_4$ cathode showed a high capacity retention of 95.15% after 150 cycles.

Keywords: Liquid alloy anodes, low surface tension, high viscosity, regulates lithium deposition, high-melting-point W nanoparticles

INTRODUCTION

With increasing demand for high energy density and excellent stability electrodes in next-generation lithium (Li) batteries, metal-based electrodes have attracted widespread attention due to their high specific capacity and outstanding electrode reaction catalytic function[1-3]. Alloy-type anode materials possessing numerous advantages with a high theoretical specific capacity, large volume energy density, low cost and moderate working potential to lithium could achieve efficient energy storage during Li alloying/dealloying, which makes them the most promising anode materials for next-generation rechargeable batteries[4-6]. Unfortunately, several problems remain, restricting their applications: (1) the inevitable volume expansion of the alloy-type anode during the lithiation process causes huge stress and strain on the material, which further causes cracking and pulverization, poor contact between the electrode materials and the current collectors; and (2) volume swelling during charge/discharge break the solid electrolyte Interphase (SEI) film on the surface of anodes, during subsequent charge/discharge cycle, the electrolyte will react with the newly exposed materials to form new SEI films, resulting in continuous consumption of electrolyte and increasing thickness of the SEI film, which will aggravate the decay of battery capacity. In efforts to address these challenges, a multitude of strategies have been proposed in the past years, involving the use of a wide variety of porous metal or liquid metal (LM)-based materials[7-11], gradient multi-porous metal electrodes[12,13], electrolyte additives[14,15], artificial SEI films[16,17], *etc.*, which have been emerged in endlessly. Especially room temperature LM-based materials[18-20] not only have the self-healing property but also alleviate the generation of Li dendrite and volume expansion during the cycle process, and they also possess a high Li storage capacity and suitable Li-alloying potential. However, the inherent disadvantages, such as fluidity and high surface tensions, restrict their spreading over most of the current collectors, resulting in a significant decline in battery life span and capacity fading; these problems have attracted extensive attention in recent years[21].

LM anodes at room temperature mainly include metallic Hg and Ga, alloys NaK, GaSn, GaIn and GaInSn, *etc.* Among them, GaInSn ternary alloys (mass ratio is 7:2:1, referred to as LM later), owing to numerous special properties including the lowest melting point (10 °C), high surface tension (718 mN/m), high electronic conductivity (3.5×10^6 S/m), low viscosity (2.4 mPa s), low toxicity, self-healing ability, and chemical stability, have been widely applied in flexible electronics, energy storage, biomedicine health, *etc.*[22-24]. Moreover, another important aspect of choosing the ternary alloy is having an "active-active-active" composite where all the elements are active with Li or alloys with Li, which enables better physical and electrochemical properties[25]. However, there is poor interfacial contact between pure LM and current collectors, and it is difficult to form a composite electrode. At present, abundant effective strategies have been put forward to improve the wettability of LM on current collectors, such as modifying current collectors[26,27] and interface decoration[28,29]. Nevertheless, related research has rarely yet been reported on changing the feature of LM itself. Thus, it is necessary to develop a new strategy to modify the fluidity and high surface tension properties of LM itself, and the inherent mechanism should be further clarified. In addition, the preparation of anodes usually will mix conductive carbon material and electron-insulating binders, which may cause the Li ion battery in the high-rate charge/discharge to encounter side reactions and larger intrinsic resistance or intangible costs, resulting in the deterioration of battery performance.

Inspired by the fact that high-melting-point metal particles mixed with LM could form an unalloyed cohesive mixture[29], we report a facial LM-W10 anode fabrication strategy by introducing tungsten (W) nanoparticles (φ 50 nm, 10 wt.%) to reducing the fluidity and surface tension of LM. After being mixed, the binder- and conductor-free LM-W10 anode presents low surface tension and high viscosity characteristics, and the composite can be easily dispersed over the current collector. A close contact interface can be thus obtained, and the reversible Li storage performance has been achieved. The present work indicates great application prospects in room temperature 3D printing manufacture of flexible devices.

EXPERIMENTAL

Materials

Gallium ingot (99.99% purity), Indium and Tin pellets (99.995% purity), and tungsten powder (99.9% purity, φ 50 nm) were purchased from Zhongnuo Advanced Material (Beijing) Technology Co., Ltd. The Cu foil (CF) was purchased through Shanghai Hesen Electrical Co., Ltd. All chemicals were used without further purification.

Preparation of materials and electrodes

The synthesis of LM (GaInSn) was carried out in an Ar-filled glove box (H_2O, O_2 < 0.1 ppm). The proportion of LM was Ga:ln:Sn = 7:2:1 (wt.%), placed in a nickel crucible, heated at 200 °C for 1 h, and constantly agitated to ensure that all components were distributed equally. The composite was collected after natural cooling. The LM and W (φ 50 nm) powders were weighed according to the mass ratio of 95:5, 90:10, 85:15, named LM-W5, LM-W10, and LM-W15, respectively, constant clockwise grinding using an agate mortar and pestle in the air until the LM form a paste-like consistency. The theoretical gravimetric capacity of the LM-W10 is 756 mAh/g (10 wt.% inactive W does not provide capacity). The commercial CF was cut into round pieces with a diameter of 14 mm, and the LM/CF, LM-W5/CF, LM-W10/CF and LM-W15/CF were fabricated to spread evenly onto the CF surface with a scraper, respectively (mass loading approximately 5 mg/cm²). In long-life symmetric cells, the Li/LM-W10/CF and Li/LM/CF were prestored with 1 or 2 mAh/cm² of Li, respectively. The pre-store process is to assemble the LM-W10/CF or LM/CF and the LM sheet into a half cell through an electrochemical deposition method; the current density is 0.5 mA/cm², and the voltage range is set to -0.01-3 V. The pre-store process of LM-W10/CF involved first conducting charge/discharge for five cycles in the half cells before depositing the amount of lithium required; however, due to the poor cycle stability of LM/CF, it can only deposit lithium directly. In full cells, the Li/LM-W10/CF and Li/LM/CF anodes were activated for one cycle at 0.1 C before long-life cycling.

Characterizations

The contact angle was tested by dropping materials on a glass slide at room temperature by a measurement instrument (JC2000D1, China). The morphology was observed by using an optical microscope (Keyence-VHX-950F) and scanning electron microscopy (SEM, Verios 460L, FEI). The surface elemental information was analyzed by an X-ray photoelectron spectrometer (XPS, ESCALAB 250Xi, ThermoFisher Scientific) and C1s (284.60 eV) as the reference line. X-ray diffraction (XRD) measurements were obtained from a Rigaku (MiniFlex 600) apparatus equipped with a Cu Kα radiation source. Cyclic voltammetry (CV) and electrochemical impedance spectroscopy (EIS) were tested by an electrochemical workstation (CHI 760E). EIS was performed at 10^5 Hz with an amplitude of 1 mV.

Battery assembly and electrochemical measurements

The electrochemical performance was carried out on CR2032. Celgard2400 was used as a separator. Symmetric cells with two identical electrodes were built; the electrolyte was 1 M lithium bis(trifluoromethanesulfonyl)imide (LiTFSI) solution in 1,3-dioxolane (DOL) and dimethoxymethane (DME) (1:1 by volume) with 1 wt.% $LiNO_3$ additive. In full cells, all anodes (Li/LM-W10/CF, Li/LM/CF, Li/CF) were prestored 0.5 mAh/cm² of Li and then assembled into full cells with $LiFePO_4$ (LFP) cathodes. The pre-store process refers to the previous section. The electrolyte was 1 M $LiPF_6$ in Ethylene carbonate/Diethyl carbonate (1:1 v/v); the cathode composition was LFP, acetylene black and Polyvinylidene fluoride at a weight ratio of 7:2:1 (mass loading 3-4 mg/cm²). The test voltage range was from 2 to 3.8 V.

RESULTS AND DISCUSSION

The LM-W5, LM-W10 and LM-W15 composites were prepared using a simple one-step grinding method. As shown in Supplementary Figure 1, the pure LM (GaInSn) displays as a liquid droplet with a metallic luster; after mixing with different mass ratio Nano-sized W powder, the LM-W5 still contains a lot of LM droplets, showing not much change in the properties of LM; however, the LM-W10 and LM-W15 form a paste that displays the characteristics of low surface tension and high viscosity. To further evaluate electrochemical performance to select the optimal W content [Supplementary Figure 2], the Li/LM-W5/CF, Li/LM-W10/CF and Li/LM-W15/CF electrodes were prestored with 1 mAh/cm^2 of Li, respectively, and assembled into symmetrical cells with two identical electrodes. The Li/LM-W5/CF exhibited a relatively high over-potential of 0.15 V and began to oscillate after 300 h, which was ascribed to high surface tension of LM-W5 leading to poor wettability with the current collector at a current density of 5 mA/cm^2. The Li/LM-W10/CF and Li/LM-W15/CF displayed a relatively low over-potential at 5 mA/cm^2; however, considering that inactive metal W does not provide capacity and cost, we select LM-W10 preferentially for the follow-up study.

As shown in Figure 1A and B, the schematic diagrams of LM-W10 and LM were presented, and contact angles were tested to investigate the wettability with current collectors. On the glass slide substrate, the contact angle of LM is 135°; by contrast, the LM-W10 could be easily spread on the glass slide, and it has strong adhesion to the substrate. Then, both LM-W10 and LM were spread on CF to fabricate LM-W10/CF and LM/CF. Observations from the optical microscope on morphology evolution [Supplementary Figure 3] show that the surface morphology of LM/CF is smooth and flat, while the LM-W10/CF is rough and convex. The mixing of W powder can completely change the physical properties of LM, thereby changing its surface tension and viscosity. According to the results of elemental distribution [Supplementary Figure 4], the W powder is evenly dispersed in LM. Figure 1C and D shows the morphology of LM-W10/CF and LM/CF after lithium deposition with different amounts. The LM-W10/CF reacts with Li smoothly, while the LM/CF surface still has a large amount of liquid droplets. With higher amount of lithium deposition, a thin and dense layer of metallic Li is deposited on the LM-W10/CF; however, the Li alloying process of LM/CF remains not optimistic, with a large amount of LM still present on electrode surface and Li alloy compounds also prone to exfoliation from the CF. Meanwhile, the SEM results also clearly revealed that the surface of LM-W10/CF after lithiation is more compact and flatter [Supplementary Figure 5A]. In sharp contrast, the LM/CF still has plenty of LM spherical droplets that are not involved in the alloying reaction after 1 mAh/cm^2 of lithiation; with the increasing amount of Li, many cracks appear in the alloying area of the electrode surface, and these alloy compounds are also easy to fall off the CF [Supplementary Figure 5B]. The main reason is the high fluidity of LM on the CF surface, and its contact with CF is not close, resulting in the detachment of Li alloy compounds from CF, while the W mixing tunes LM wettability, giving LM-W10 a stronger adhesion on CF, thus forming a complete structure. It makes the charge transfer between the CF and the electrode material more rapid and stable, homogenizing Li ion transfer flux of the anode surface and making the Li alloy compounds more uniform and denser. Additionally, it demonstrates that we have successfully developed a new conductive-binder-free anode of LM-W10/CF. To verify whether the W mixing will affect self-healing nature of the LM, the morphological changes during lithiation/delithiation of the LM-W10/CF were observed by SEM. The pristine electrode surface was observed to have an even layer of LM-W10, as shown in Supplementary Figure 6A. After full lithiation, the surface of LM-W10 alloy compounds is more compact and flatter [Supplementary Figure 6B]. The SEM image in Supplementary Figure 6C displays the formation of numerous consistent, smaller and glittery LM-W10 spherical particles after the delithiation process with some of the delithiation LM-W10 micro-particles also exhibiting a deformed shape, and the elemental distribution also further verifies the formation of liquid droplet LM-W10 [Supplementary Figure 6C0-C4]; these results indicate that the metal mixing strategy has a negligible effect on the self-healing nature of LM.
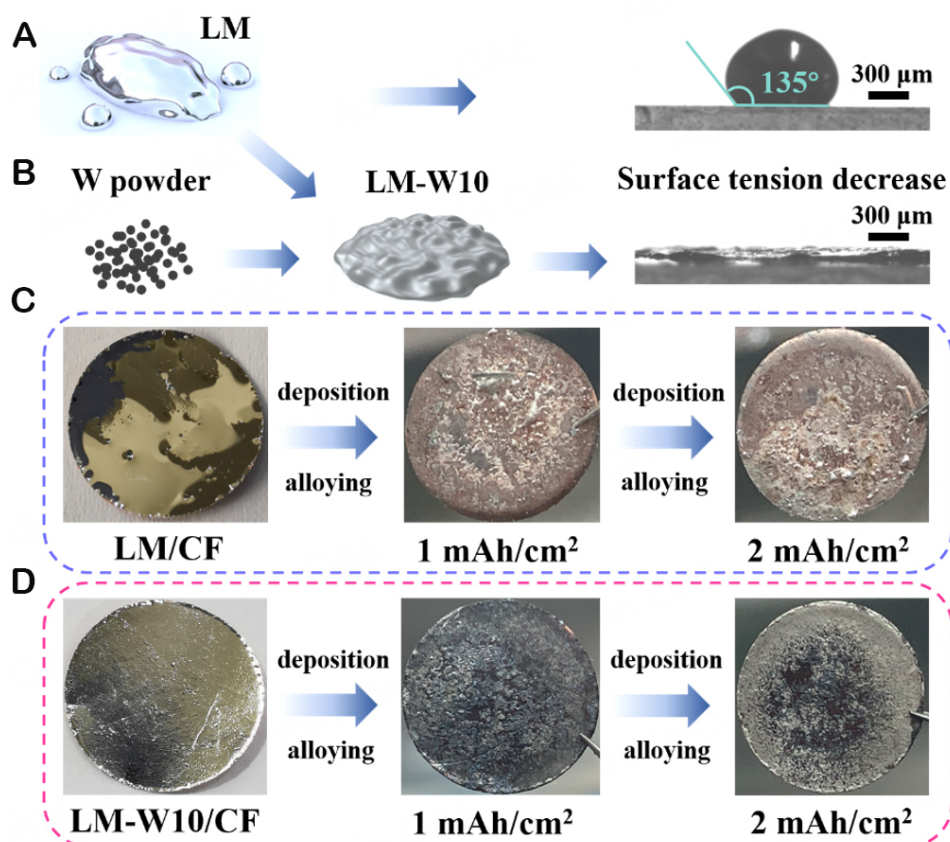
Figure 1. The schematic diagram of (A) LM and (B) LM-W10, and corresponding contact angles on glass slide; optical microscopy photos of (C) LM/CF and (D) LM-W10/CF after lithiation at a current density of 1 mA/cm^2.

It is vital to understand the Li alloying/dealloying process of LM-W10/CF and LM/CF for further performance optimization. The XRD patterns were recorded to analyze the phase composition [Supplementary Figure 7A]. It can be concluded that, for both LM-W10/CF and LM/CF, the broad peaks at around 35° belong to amorphous LM, and the sharp peaks at 43.18°, 50.30° and 74.05° are assigned to CF. After lithiation, obvious GaLi peaks at 24.74°, 41.27°, 48.59° and 75.45° were observed in Li/LM-W10/CF, which well matched with the characteristic peaks of GaLi (JCPDS 09-0043); also, weak lnLi peaks at 22.63°, 37.36°, and 43.98° were observed, which are consistent with the characteristic peaks of lnLi (JCPDS 65-5507). In addition, we found a small amount of CuGa$_2$ (JCPDS 25-0275). The reason for the generation of CuGa$_2$ is mainly due to the non-solid phase gallium-based alloys forming alloys with CF. Moreover, the formation of the CuGa$_2$ layer will also significantly reduce the nucleation potential barrier with Li and homogenize the mass transfer flow of Li$^+$ on the anode surface[19]. The formation of new compounds of W is not observed, which means that Nano-sized W powder is very stable, and no new phases were formed during the reaction. Add the nano-sized W powder into the electrolyte (without salt) and stirred it continuously at room temperature for different durations [Supplementary Figure 7B]. It demonstrates that the diffraction peak of W has almost not changed, and as shown in Supplementary Figure 7C and D, the results showed that the CV curves of carbon paper with W powder were the same as those of carbon paper. It further shows that W powder is not involved in the electrochemical reaction and that W powder is much more stable in the electrolyte. The CV was conducted in the voltage range from 0.01 to 2 V. As shown in Figure 2A, for LM-W10/CF, four couple of redox peaks at 0.71/0.95, 0.54/0.78, 0.43/0.71, and 0.27/0.49 V in one full cycle are associated with the lithiation/delithiation of Ga, Sn/In, Ga, and Sn, respectively[30,31]. By contrast, for LM/CF, no obvious or weak redox peaks are found during cycles, which should be attributed to
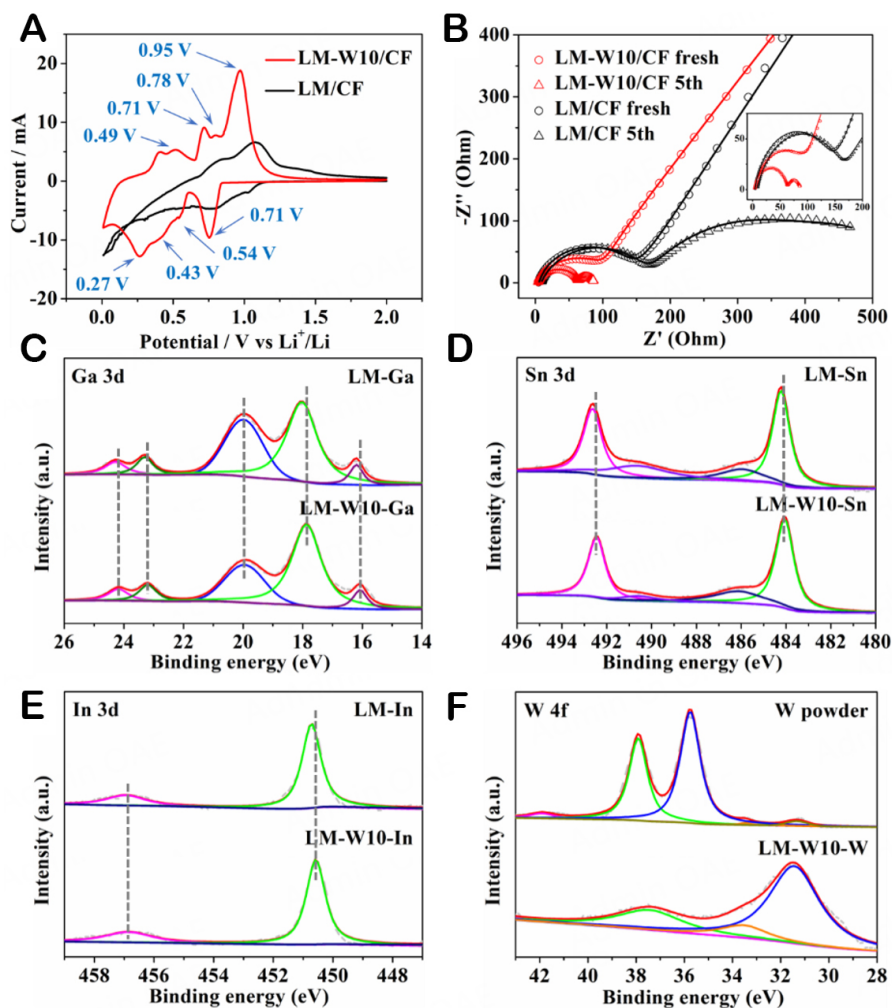
Figure 2. (A) The cyclic voltammetry of LM-W10/CF and LM/CF at 0.5 mV/s; (B) Nyquist plots of fresh and after five cycles of Li||LM-W10/CF and Li||LM/CF in half cells (The inset is an enlarged image); (C-F) XPS spectra comparison of different elements (Ga 3d, Sn 3d, In 3d and W 4f).

the large electrode polarization and poor interfacial contact. The LM-W10 alloy with high viscosity and low surface tension reduces the activity of Li in the solid phase and homogenizes the flux of Li$^+$ ions to the electrode surface. In the subsequent cycles [Supplementary Figure 8], the peaks can coincide well, which indicates the fast stabilization of anode interface layers and perfect cycling stability during repeated lithiation/delithiation. EIS measurement of half cells was performed to evaluate electrode interfacial reaction [Figure 2B]. Whether before cycle or after five cycles, the overall cell impedance value of Li||LM-W10/CF is less than that of Li||LM/CF. Especially after cycling, the charge transfer resistance and interfacial impedance of Li$^+$ ions through the SEI film of LM-W10/CF become much smaller compared to LM/CF, which is mainly attributed to the effective interface contact properties of LM after mixing with W powder, thereby optimizing the ion/electron transfer rate[20]; this is in good agreement with the results in Figure 2A and Supplementary Figure 8. Meanwhile, the equivalent circuit models of LM-W10/CF and LM/CF batteries are shown in Supplementary Figure 9. The resistance values of the LM-W10/CF were smaller than those of the LM/CF. It also indicates that the interface and charge transfer resistance inside the battery is much lower, which is attributed to the high viscosity and low surface tension of LM-W10, which enables it to maintain a good contact interface with the CF, thus exhibiting excellent electrochemical performance. The X-ray

photoelectron spectroscopy (XPS) was used to disclose the chemical state of LM in the composite anode. As shown in Figure 2C-E, the XPS peak patterns of Ga 3d, Sn 3d and ln 3d in LM-W10/CF and LM/CF are almost identical; however, some peak positions of LM-W10/CF are shifted by about 0.14 or 0.21 eV towards the lower binding energy compared to LM/CF (all XPS spectra have been corrected with C1s 284.6 eV). For the W 4f spectrum in Figure 2F, all peak positions shift more significantly, and the half-peak width is larger; the peaks at 37.91 and 35.77 eV are shifted towards the low binding energy by about 0.45 and 4.31 eV, respectively. It indicates that the electronegativity of W increased after composing with LM. Considering the difference in the electronegativity of W (2.36) > Sn (1.96) > Ga (1.81) > ln (1.78). The charge localization of GaInSn alloy is weakened after the introduction of strong electronegativity metal W, resulting in the presence of binding energy shifts. This means that electrons from the GaInSn atoms were transferred to the W atoms, the electron cloud density around the W atoms will increase when W gets a large number of electrons, and the binding energy will obviously decrease accordingly. The slight shift of each element in GaInSn towards the direction of low binding energy may be due to the mixing of W atoms and GaInSn forming a whole. Although the difference of their electronegativity will lead to charge transfer, the overall electron cloud density will increase[32-35].

To evaluate the electrochemical performance of the Li/LM-W10/CF and Li/LM/CF anode, symmetric cells were assembled to study the reversible Li storage performance. As shown in Figure 3A, both electrodes were deposited with 1 mAh/cm² of Li and assembled into symmetrical cells with two identical electrodes, then fixed areal capacity of 0.5 mAh/cm² in subsequent repeated cycles. The Li/LM-W10/CF displayed a relatively low over-potential (~13 mV) and remained stable for more than 8,000 h (4,000 cycles) at a current density of 0.5 mA/cm². Meanwhile, the Li/LM/CF exhibited an over-potential of ~28 mV, and short-circuit occurred after about 3,700 h (~1,850 cycles). Figure 3B shows the performance of samples prestored with 2 mAh/cm² of Li and a fixed areal capacity of 1 mAh/cm². The Li/LM-W10/CF showed a low over-potential (~27 mV) with a cycle life for more than 8,000 h (4,000 cycles) at 1 mA/cm², while the Li/LM/CF exhibited a high over-potential of ~39 mV and began to oscillate at 3,400 cycles. This might be caused by non-uniform lithiation processes and serious SEI accumulation. The Li/LM-W10/CF has a lower lithiation over-potential (13.4 mV) than that of the Li/LM/CF (20.2 mV) in Figure 3C. And the rate performance of the Li/LM-W10/CF symmetric battery was further explored [Figure 3D]; the voltage hysteresis increases slightly from 7 to 30 mV with the increase of the current density from 0.2 to 1 mA/cm². The above results demonstrate that the cycling stability and lithiation over-potential of Li/LM-W10/CF is better than that of Li/LM/CF, which is benefited by the excellent interfacial contact and superior electrochemical kinetics between CF and Li/LM-W10.

The Li/LM-W10/CF anode was fabricated into full cells coupled with LFP cathodes to investigate its practical applications. Figure 4A shows the cycling performance of full cells with different anodes at 1C. The Li/LM-W10/CF||LFP cell presents outstanding stability and maintains at 144 mAh/g with an average Coulombic Efficiency (CE) of 98.9%. The capacity retention is 95.15% even after 150 cycles with a fading rate of only 0.032% per cycle. By contrast, the discharge capacities of the Li/LM/CF||LFP and Li/CF||LFP cells rapidly decayed after 110 and 90 cycles, with relatively low CEs of 94.6% and 92.4%, respectively. The performance degradation of Li/LM/CF||LFP and Li/CF||LFP full cells is associated with the poor interfacial contact between originally low content of Li alloy compound and CF surface, which may lead to a "soft short circuit" within the battery. The poor contact also results in large electrode polarization and Li consumption in the subsequent cycle, thus deteriorating the life span of the battery. Supplementary Figure 10 disclosed the corresponding charge/discharge voltage profiles for the Li/LM-W10/CF||LFP full cell at different cycles. The specific discharge capacities of Li/LM-W10/CF||LFP were 151.8, 141.4, 139.1, and 130.2 mAh/g at 0.2, 0.5, 0.8, and 1C, respectively [Figure 4B], indicating stable charge/
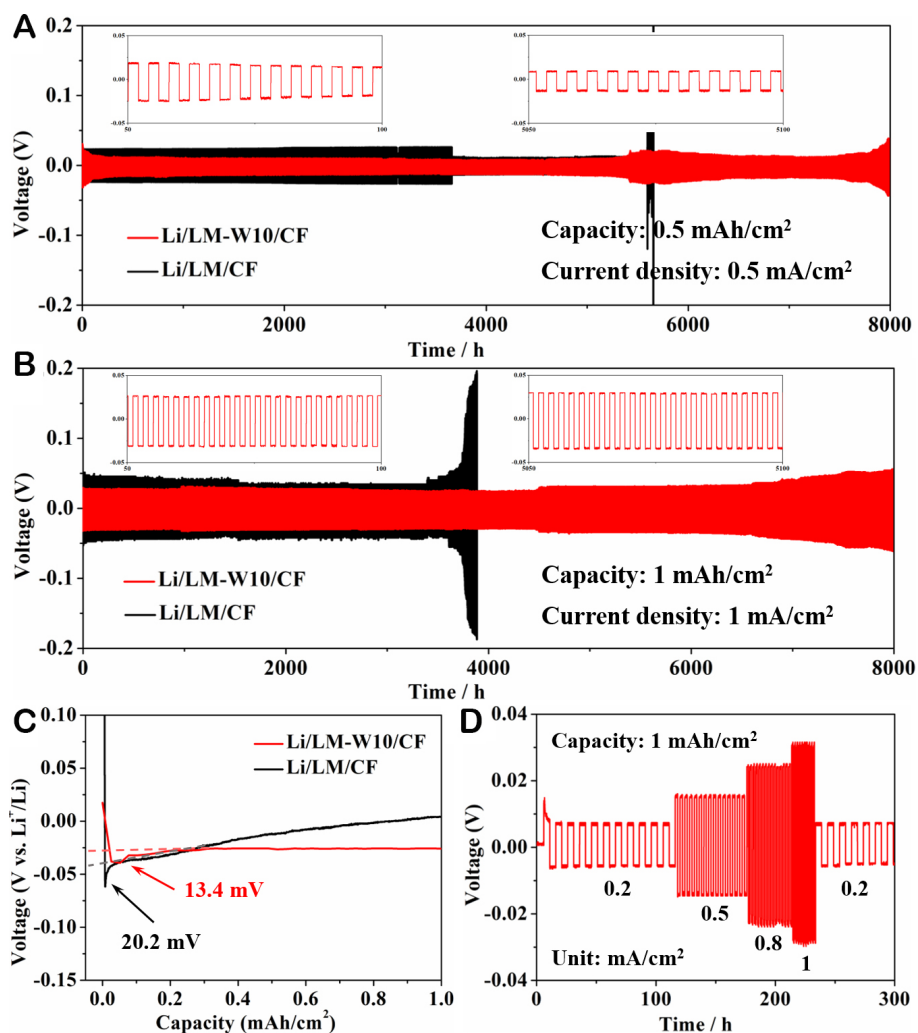
Figure 3. Electrochemical performance of symmetric cells with Li/LM-W10/CF and Li/LM/CF. (A and B) the current densities were controlled to be 0.5 and 1 mA/cm^2 (The inset were enlarged time-voltage curves); (C) nucleation over-potentials for lithiation in the three electrodes model cell at ~ 1 mA/cm^2; (D) rate performance of Li/LM-W10/CF from 0.2 to 1 mA/cm^2 (2 mAh/cm^2 pre-deposited Li).
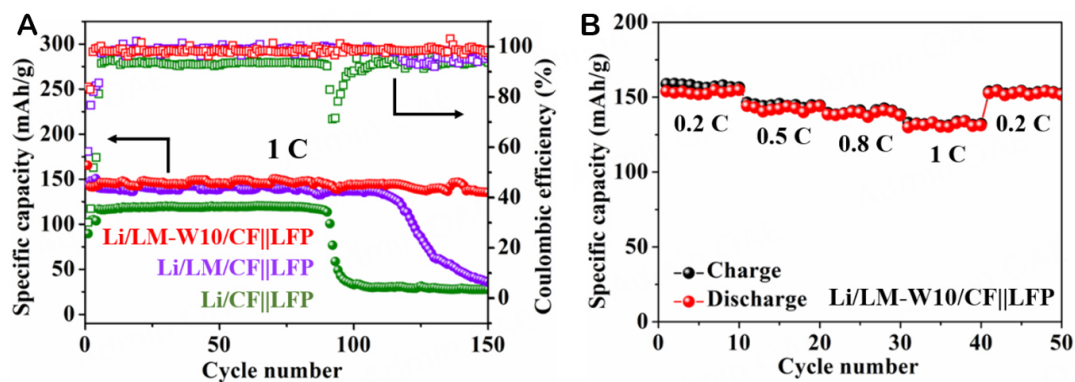

Figure 4. (A) Cycling performances of Li/LM-W10/CF||LFP, Li/LM/CF||LFP, and Li/CF||LFP full cell at 1C (1C = 170 mA/g); (B) rate performance of Li/LM-W10/CF||LFP full cell.

discharge rate performance. As previously discussed, it is precisely because the metal mixing strategy forms an electrode with a close contact interface and stable charge/ion transport that homogenizes the local current density and improves the CEs of the cells.

CONCLUSIONS

In summary, a new binder- and conductor-free anode of LM-W10/CF was developed by one-step simple painting strategy. The introduction of high-melting-point W nanoparticles could effectively decrease the fluidity and surface tension of LM and make it easy to spread evenly over the current collector; the strategy has a negligible effect on the self-healing nature of LM. It greatly improves the inherent defects of poor interfacial contact and Li diffusion kinetics between the LM and current collectors, regulates lithium deposition behaviors, enhances the safety of LM anodes to a great extent and reduces the tedious and costly electrode manufacturing process, which makes this LM-W10/CF more suitable in the field of flexible electronic equipment. The LM-W10/CF composite electrode showed a low over-potential (~13 mV) and maintained cycle stability for more than 8,000 h (4,000 cycles) at 0.5 or 1 mA/cm^2 in symmetric cells. Moreover, full cell tests upon pairing LFP cathodes demonstrated excellent cycling stability and rate properties and maintained a high-capacity retention of 95.15% after 150 cycles. Utilizing this ingenious and facile technology can definitely further improve the energy density of the LM anode and produce it in mass production. Furthermore, it is also appropriate for other alkali metal anodes[36-38] (e.g., Na and K) and will greatly expand the application field of flexible batteries in the future.

DECLARATIONS

Authors' contributions
Materials synthesis, condition optimization, manuscript writing, electrochemical experiment testing and analysis: Lv Y
Intellectual contribution: Hu H
Acquired funding, supervised and guided the entire work, and made a major contribution to the writing and flow of the manuscript: Liu X

Availability of data and materials
Not applicable.

Conflicts of interest
All authors declared that there are no conflicts of interest.

Ethical approval and consent to participate
Not applicable.

Consent for publication
Not applicable.

REFERENCES

1.　Liu H, Liu X, Wang S, Liu H, Li L. Transition metal based battery-type electrodes in hybrid supercapacitors: a review. *Energy Stor Mater* 2020;28:122-45.　DOI

2.　Xie J, Lu YC. A retrospective on lithium-ion batteries. *Nat Commun* 2020;11:2499.　DOI　PubMed　PMC

3.　Shen X, Liu H, Cheng XB, Yan C, Huang JQ. Beyond lithium ion batteries: higher energy density battery systems based on lithium metal anodes. *Energy Stor Mater* 2018;12:161-75.　DOI

4.　Ni J, Zhu X, Yuan Y, et al. Rooting binder-free tin nanoarrays into copper substrate via tin-copper alloying for robust energy storage. *Nat Commun* 2020;11:1212.　DOI　PubMed　PMC

5.　Li Q, He G, Ding Y. Applications of low-melting-point metals in rechargeable metal batteries. *Chemistry* 2021;27:6407-21.　DOI

6.　Shi Y, Yang W, Bai Q, Qin J, Zhang Z. Alloying/dealloying mechanisms, microstructural modulation and mechanical properties of nanoporous silver via a liquid metal-assisted alloying/dealloying strategy. *J Alloys Compd* 2021;872:159675.　DOI

7.　Chi SS, Wang Q, Han B, et al. Lithiophilic Zn sites in porous CuZn alloy induced uniform Li nucleation and dendrite-free Li metal deposition. *Nano Lett* 2020;20:2724-32.　DOI

8.　Yu J, Xia J, Guan X, et al. Self-healing liquid metal confined in carbon nanofibers/carbon nanotubes paper as a free-standing anode for flexible lithium-ion batteries. *Electrochim Acta* 2022;425:140721.　DOI

9.　Yun J, Park BK, Won ES, et al. Bottom-up lithium growth triggered by interfacial activity gradient on porous framework for lithium-metal anode. *ACS Energy Lett* 2020;5:3108-14.　DOI

10.　Won P, Jeong S, Majidi C, Ko SH. Recent advances in liquid-metal-based wearable electronics and materials. *iScience* 2021;24:102698.　DOI　PubMed　PMC

11.　Jia H, Wang Z, Dirican M, et al. A liquid metal assisted dendrite-free anode for high-performance Zn-ion batteries. *J Mater Chem A* 2021;9:5597-605.　DOI

12.　Lv Y, Zhang QX, Li C, et al. Bottom-up Li deposition by constructing a multiporous lithiophilic gradient layer on 3D Cu foam for stable Li metal anodes. *ACS Sustain Chem Eng* 2022;10:7188-95.　DOI

13.　Hyun G, Cao S, Ham Y, et al. Three-dimensional, submicron porous electrode with a density gradient to enhance charge carrier transport. *ACS Nano* 2022;16:9762-71.　DOI

14.　Park S, Jeong SY, Lee TK, et al. Replacing conventional battery electrolyte additives with dioxolone derivatives for high-energy-density lithium-ion batteries. *Nat Commun* 2021;12:838.　DOI　PubMed　PMC

15.　Ming J, Cao Z, Wu Y, et al. New insight on the role of electrolyte additives in rechargeable lithium ion batteries. *ACS Energy Lett* 2019;4:2613-22.　DOI

16.　Meda US, Lal L, M S, Garg P. Solid electrolyte interphase (SEI), a boon or a bane for lithium batteries: a review on the recent advances. *J Energy Stor* 2022;47:103564.　DOI

17.　Liu W, Liu P, Mitlin D. Solid electrolyte interphases: review of emerging concepts in SEI analysis and artificial SEI membranes for lithium, sodium, and potassium metal battery anodes. *Adv Energy Mater* 2020;10:2070177.　DOI

18.　Wu Y, Huang L, Huang X, et al. A room-temperature liquid metal-based self-healing anode for lithium-ion batteries with an ultra-long cycle life. *Energy Environ Sci* 2017;10:1854-61.　DOI

19.　Meng J, Li C. Planting CuGa$_2$ seeds assisted with liquid metal for selective wrapping deposition of lithium. *Energy Stor Mater* 2021;37:466-75.　DOI

20.　Guo X, Zhang L, Ding Y, Goodenough JB, Yu G. Room-temperature liquid metal and alloy systems for energy storage applications. *Energy Environ Sci* 2019;12:2605-19.　DOI

21.　Wei C, Tan L, Zhang Y, et al. Review of room-temperature liquid metals for advanced metal anodes in rechargeable batteries. *Energy Stor Mater* 2022;50:473-94.　DOI

22.　Yang Z, Yang D, Zhao X, et al. From liquid metal to stretchable electronics: overcoming the surface tension. *Sci China Mater* 2022;65:2072-88.　DOI

23.　Yan J, Lu Y, Chen G, Yang M, Gu Z. Advances in liquid metals for biomedical applications. *Chem Soc Rev* 2018;47:2518-33.　DOI

24.　Han B, Xu D, Chi SS, et al. 500 Wh kg^{-1} class Li metal battery enabled by a self-organized core-shell composite anode. *Adv Mater* 2020;32:e2004793.　DOI

25.　Sengupta S, Patra A, Akhtar M, Das K, Majumder SB, Das S. 3D microporous Sn-Sb-Ni alloy impregnated Ni foam as high-performance negative electrode for lithium-ion batteries. *J Alloys Compd* 2017;705:290-300.　DOI

26.　Ozutemiz KB, Wissman J, Ozdoganlar OB, Majidi C. EGaIn-Metal interfacing for liquid metal circuitry and microelectronics integration. *Adv Mater Inter* 2018;5:1701596.　DOI

27.　Ding Y, Guo X, Qian Y, Xue L, Dolocan A, Yu G. Room-temperature all-liquid-metal batteries based on fusible alloys with regulated interfacial chemistry and wetting. *Adv Mater* 2020;32:e2002577.　DOI

28.　Wei C, Tan L, Tao Y, et al. Interfacial passivation by room-temperature liquid metal enabling stable 5 V-class lithium-metal batteries in commercial carbonate-based electrolyte. *Energy Stor Mater* 2021;34:12-21.　DOI

29.　Kong W, Wang Z, Wang M, et al. Oxide-mediated formation of chemically stable tungsten-liquid metal mixtures for enhanced thermal interfaces. *Adv Mater* 2019;31:e1904309.　DOI

30.　Guo X, Ding Y, Xue L, et al. A self-healing room-temperature liquid-metal anode for alkali-ion batteries. *Adv Funct Mater* 2018;28:1804649.　DOI

31.   Wei C, Fei H, Tian Y, et al. Room-temperature liquid metal confined in MXene paper as a flexible, freestanding, and binder-free anode for next-generation lithium-ion batteries. *Small* 2019;15:e1903214. DOI

32.   Yu S, Kaviany M. Electrical, thermal, and species transport properties of liquid eutectic Ga-In and Ga-In-Sn from first principles. *J Chem Phys* 2014;140:064303. DOI PubMed

33.   Zhang Q, Lei X, Lv Y, Ma C, Liu X. Liquid metal-based cathode for flexible ambient Li-air batteries and its regeneration by water. *Appl Surf Sci* 2023;607:155074. DOI

34.   Savu SA, Casu MB, Schundelmeier S, et al. Nanoscale assembly, morphology and screening effects in nanorods of newly synthesized substituted pentacenes. *RSC Adv* 2012;2:5112-8. DOI

35.   Chao D, Ye C, Xie F, et al. Atomic engineering catalyzed MnO_2 electrolysis kinetics for a hybrid aqueous battery with high power and energy density. *Adv Mater* 2020;32:2001894. DOI

36.   Tang S, Song F, Lu M, Han K, Peng X. Rational design of a visible-light photochromic diarylethene: a simple strategy by extending conjugation with electron donating groups. *Sci China Chem* 2019;62:451-9. DOI

37.   Wang C, Wang L, Li F, Cheng F, Chen J. Bulk bismuth as a high-capacity and ultralong cycle-life anode for sodium-ion batteries by coupling with glyme-based electrolytes. *Adv Mater* 2017;29:1702212. DOI

38.   Fu M, Zhang X, Dong W, et al. Optimizing Na plating/stripping by a liquid sodiophilic Ga-Sn-In alloy towards dendrite-poor sodium metal anodes. *Energy Stor Mater* 2023;63:103020. DOI